Int. J. Electrochem. Sci., 6 **(2011)** 442 - 460

International Journal of
ELECTROCHEMICAL
SCIENCE
www.electrochemsci.org

Influence of Sensitisation on the Corrosion Behaviour of Alloy 926 (UNS N08926) in Concentrated Aqueous Lithium Bromide Solutions at Different Temperatures

R. Leiva-García, M. J. Muñoz-Portero, J. García-Antón[*]

Ingeniería Electroquímica y Corrosión (IEC)
Departamento de Ingeniería Química y Nuclear, E.T.S.I. Industriales,
Universidad Politécnica de Valencia E-46071 Valencia, Spain
[*]E-mail: jgarciaa@iqn.upv.es

Received: 26 November 2010 / *Accepted:* 25 December 2010 / *Published:* 1 February 2011

The aim of this work is to study the influence of sensitisation to intergranular corrosion on a highly alloyed austenitic stainless steel, Alloy 926 (UNS N08926). Some specimens of this steel have been heated in an argon atmosphere at 825 ºC during 1 hour. The degree of sensitisation has been characterised by means of SEM, etching (with oxalic acid), and electrochemical reactivation methods (single and double loop tests). The corrosion behaviour of sensitised and unsensitised Alloy 926 has been analysed in a concentrated aqueous lithium bromide (LiBr) solution of 992 g/L by means of cyclic potentiodynamic curves at different temperatures. The results indicate that chromium carbide precipitates reduce the pitting potential value of Alloy 926. Besides, the pitting potential decreases with temperature. On the other hand, the corrosion potential and open circuit potential values increase with temperature and sensitisation.

Keywords: Stainless steel, intergranular corrosion, pitting, sensitisation.

1. INTRODUCTION

Refrigeration absorption machines are again considered as suitable refrigeration systems because the use of chlorofluorocarbons (CFCs) was banned (Montreal Protocol [1], 1987) and their substitutes, i.e. hydrochlorofluorocarbons, are submitted to severe regulations, Kyoto protocol [2], 1997). Absorption machines can use different working fluids, such as (NH_3-H_2O) or (H_2O-LiBr). The last one, H_2O-LiBr, is the most commonly employed refrigerant/absorbent couple in absorption systems due to their favourable thermophysical properties [3, 4]. However, LiBr can cause serious corrosion problems on metallic components in refrigeration systems. Bromides, like chlorides, are

aggressive ions and their corrosion effect may be accelerated in absorption machines due to the high temperatures and concentrations reached in them. Therefore, stainless steels are widely used in structural elements because they present good corrosion resistance. The corrosion resistance of stainless steel is mainly due to its chromium content because a chromium oxide film is formed that protects the alloy [5-7]. AISI 304 and AISI 316 austenitic stainless steels are the most commonly manufactured materials. However, in austenitic stainless steels, an improper heat treatment in the temperature range between 500 and 900 ºC causes chromium and carbon to react at grain boundaries and form chromium carbides, concomitant with the formation of chromium depletion zones appear at the adjacent zones [8-23]. Then, the corrosion resistance of the steels decreases as a result of the precipitation of chromium carbides. The high concentration of chromium in $Cr_{23}C_6$ particles, which is one of the most stable carbides [24, 25], reduces locally the chromium content in the region adjacent to these chromium rich precipitates. Since chromium diffuses much more slowly than carbon, there is not enough time for chromium to diffuse to the carbide from all over the grains. So, in the region that is near grain boundaries, the chromium content lowers below 13 %, which is a critical value for the corrosion resistance of stainless steels. This process that forms a chromium depletion zone is called sensitisation to intergranular corrosion. Various evaluation tests have been developed to determine the susceptibility of stainless steels to intergranular attack. Some of them are described in standard ASTM A – 262 [26]. Furthermore, there are electrochemical potentiokinetic reactivation tests (EPR) (single and double loop) [21, 27-30] that permit evaluating the degree of sensitisation (DOS).

Several papers have studied the corrosion in LiBr solutions [3, 31-38]. In a previous work, the corrosion behaviour of a duplex stainless steel in concentrated aqueous LiBr solutions was studied in its as-received and sensitised state [39]. In that case, sensitisation process was due to the formation of new phases. Therefore, the aim of this work is the study of the sensitisation influence over the corrosion behaviour of a highly alloyed austenitic stainless steel Alloy 926 (UNS N08926) in concentrated aqueous LiBr solutions at different temperatures (25 ºC, 50 ºC, and 75 ºC). This stainless steel has a higher content in nickel and molybdenum than conventional austenitic stainless steels, such as AISI 304 or AISI 316. This higher nickel and molybdenum content gives substantially improved resistance to pitting and crevice corrosion in halide media. As a result, Alloy 926 can be considered an interesting material in absorption machines that use aggressive LiBr solutions.

2. EXPERIMENTAL PROCEDURE

2.1. Materials

A highly alloyed austenitic stainless steel, Alloy 926 (UNS N08926) supplied by Krupp, was used in the electrochemical tests. The chemical composition in weight of Alloy 926 is: 20.8 % Cr, 24.90 % Ni, 0.90 % Mn, 0.35 % Si, 6.45 % Mo, 0.94 % Cu, 45.16 % Fe, 0.02 % P, 0.01 % C, and 0.18 % N. The electrodes of Alloy 926 were machined and shaped as a rectangular prism 30 mm high with a base surface of 0.36 cm^2.

Three specimens of Alloy 926 were introduced in a silica tube in a furnace (CARBOLITE TVS 12/600) under an argon atmosphere. The furnace was controlled by the software "*iTools*" provided by "Eurotherm". Then, the specimens were heated to develop sensitisation. Heat treatments were carried out at 825 ºC for a period of 1 hour. These conditions were selected because in previous works, sensitisation was observed with this heat treatment [40, 41]. Finally, the specimens were water quenched. After the heat treatment, the specimens were covered with polytetrafluorethylene coating. In this way, only an area of 0.36 cm^2 was exposed to the solution. Prior to the electrochemical tests, the specimens were wet abraded from 220 SiC (Silicon Carbide) grit to a 4000 SiC grit finish, and finally rinsed with distilled water.

2.2. Sensitisation characterisation

Single and Double Loop Reactivation Potentiokinetic tests were applied in order to characterise the degree of sensitisation of Alloy 926. The electrolyte employed for the reactivation tests was 2 M H_2SO_4, 0.01M KSCN, and 0.5 M NaCl [42, 43]. In the single loop method, the specimen was passivated at 200 mV vs saturated calomel electrode (240 mV vs Ag/AgCl with 3M KCl electrode) for two minutes. Later, the potential decreased down to the open circuit potential at 1.667 mV/s. A measure of the degree of sensitisation could be obtained by calculating the reactivation charge [30]. In the double loop method, the Open Circuit Potential (OCP) was measured for two minutes. Next, the work electrode was anodically polarised from OCP to 300 mV vs saturated calomel electrode (340 mV vs Ag/AgCl with 3M KCl electrode) at a rate of 1.667 mV/s; this is the activation loop. Then, the scanning direction was reversed and the potential decreased at the same rate until reaching OCP; this is the reactivation loop. The ratio between charges in the reactivation (Qr) and activation (Qa) loop was used to measure the degree of sensitisation (DOS).

$$DOS(\%) = Qr / Qa \qquad (1)$$

The specimens could be classified into different levels of sensitisation (unsensitised, slightly sensitised, medium sensitised or severely sensitised) depending on their sensitisation degree and reactivation charge using different correlations, such as the standard ASTM G-108 or Cihal proposed in the literature [30, 44].

2.3. Microscopic analysis

In order to estimate the formation of chromium carbides during the heat treatment, the materials were examined by scanning electron microscopy (SEM) and backscattered electrons. In addition, the materials were etched according to ASTM A-262 [26] with oxalic acid to reveal chromium carbides

2.4. Cyclic Potentiodynamic Curves

The specimens of unsensitised and sensitised Alloy 926 were tested in 992 g/L LiBr aqueous solutions at different temperatures: 25 ºC, 50 ºC, and 75 ºC. LiBr solutions were prepared from LiBr (minimum purity of 98 %) provided by "*Panreac*" company.

Cyclic Potentiodynamic Curves were determined using a Solartron 1287. In all cases, the tests were repeated at least three times. The scans presented in this paper show one of the curves obtained. The devices P-200002525 and P-200002526 [45-48] were employed in the electrochemical tests. These devices allow observing the electrode surface in real-time as it undergoes electrochemical corrosion processes. The experimental devices consist of two elements: the electrochemical unit and the image acquisition section. The electrochemical system is composed of the data acquisition equipment, which registers the electrical signal obtained from the corrosion processes that take place inside a horizontal electrochemical cell. The image acquisition system consists of a microscope-stereoscope and a colour video camera assembled to the optical device.

The potentials of the working electrode were measured against a silver-silver chloride with 3M KCl reference electrode. The auxiliary electrode was a platinum electrode. Polarisation curves were obtained in deaireated LiBr aqueous solution by bubbling nitrogen for 25 minutes, prior to immersion. During the test, a nitrogen atmosphere was maintained over the liquid surface. Before each polarisation test, the specimen was immersed in the test solution for 1 hour at the open circuit potential (OCP). After the OCP test, the specimen potential was reduced progressively to -1000 $mV_{Ag/AgCl}$ during 60 seconds in order to create reproducible initial conditions. Then, the potentiodynamic curves were recorded from – 1000 $mV_{Ag/AgCl}$ to anodic direction at 0.1667 mV/s sweep rate. When the current density reached 10 mA/cm^2, the potential scan was reversed in order to evaluate the repassivation tendency of the metal.

3. RESULTS AND DISCUSSION

3.1. Microscopic analysis

Figure 1 shows the image of a sensitised specimen of Alloy 926 obtained by SEM and backscattered electrons. In this figure, chromium carbides are brighter than the rest of the surface due to their higher chromium content. These carbides are surrounding the grain boundaries of austenite. On the other hand, chromium carbides were revealed by etching them with oxalic acid in order to verify the results obtained with the SEM analysis. Figure 2 shows the unsensitised and sensitised Alloy 926 after etching with oxalic acid. The unsensitised specimen shows no attack around the grain boundaries, whereas the sensitised specimen shows a ditch structure, where all the grains are completely surrounded by an attacked area.

Therefore, after the microscopic study, it is clear that the sensitisation process produces chromium carbide precipitation at the grain boundaries. The precipitation of chromium carbides results in chromium depletion in the neighbouring areas. Despite the fact that the carbon content is lower than

0.03 % (limit that is generally established to avoid the carbide precipitation [49]) chromium carbides appears because carbon solubility is considerably lower and chromium diffusion is faster in nickel-base alloys and austenitic stainless steels with high nickel content [50]. On the other hand, it can be expected that the areas close to the chromium carbides become sensitised to intergranular corrosion.

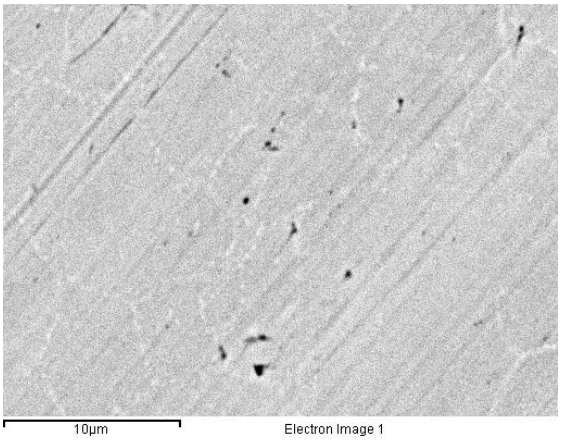

Figure 1. Image of sensitised Alloy 926 obtained by scanning electron microscopy and backscattered electrons. Chromium carbides are brighter than the rest of the surface.

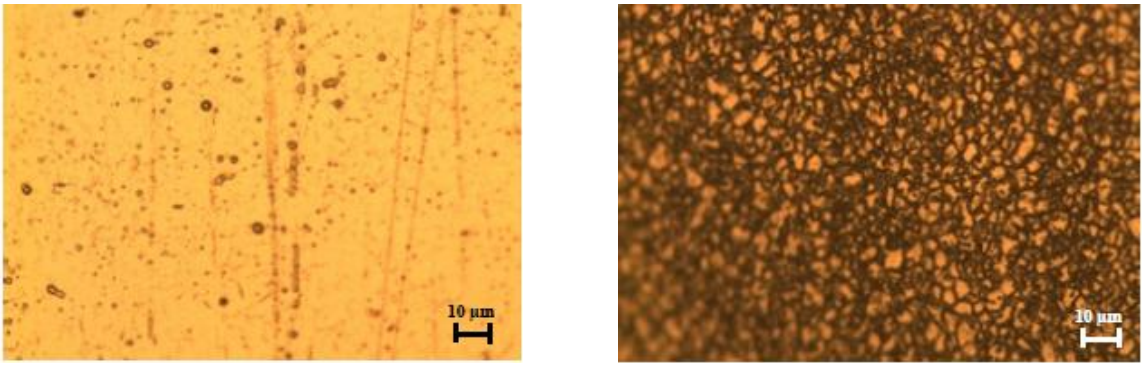

a) Unsensitised Alloy 926 b) Sensitised Alloy 926

Figure 2. Images of unsensitised and sensitised Alloy 926 after etching with oxalic acid.

3.2. Sensitisation characterisation

Figure 3 shows the single and the double loop curves for unsensitised Alloy 926 and Alloy 926 sensitised at 825 ºC.

According to the results of the single loop test, the sensitised sample shows a higher reactivation charge than the unsensitised sample, as shown in Figure 3 a. The charge values of unsensitised and sensitised Alloy 926 were 0.02 C/cm^2 and 0.43 C/cm^2, respectively. There is a noticeable increase in the reactivation charge as a consequence of the heat treatment. According to the reactivation charge and the correlations proposed in the literature [30], heated Alloy 926 is severely sensitised.

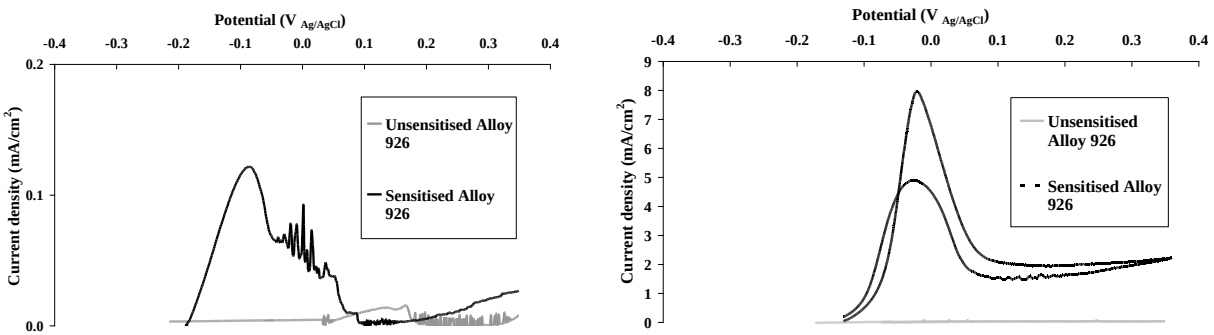

a) Single Loop tests b) Double Loop tests

Figure 3. Single and Double loop curves for unsensitised Alloy 926 and Alloy 926 sensitised at 825 ºC for 1 hour.

In the case of the double loop test, results show that heat treatment increases the degree of sensitisation detected during the electrochemical reactivation tests. The DOS value of non heated and heated Alloy 926 is 0.0 % and 60.76%, respectively. The results obtained by means of the double loop method indicates a high level of sensitisation as reported by Cihal [44]. Furthermore, in the double loop curves, it can be observed that both the reactivation and activation charge increase as a consequence of heat treatment. The increase in the activation and reactivation charge is related with a weaker passive film in the areas with a lower chromium content. Therefore, the chromium carbides observed in the microscopic analysis have a great influence on the corrosion behaviour of Alloy 926.

3.3 Open circuit potentials

The OCP values of unsensitised and sensitised Alloy 926 in the 992 g/L LiBr aqueous solution at the different temperatures are shown in Figure 4.

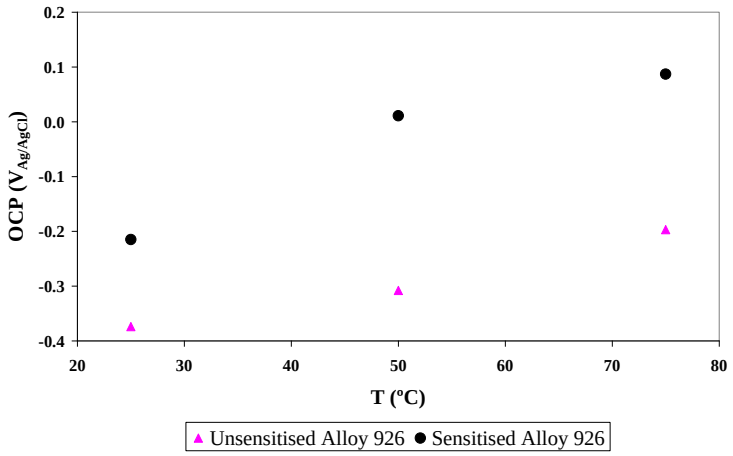

Figure 4. Open Circuit Potential values of unsensitised and sensitised Alloy 926 in the 992 g/L LiBr solution at different temperatures.

The highest OCP values are exhibited by the sensitised sample. The maximum value of the OCP has been obtained in the sensitised material at 75 ºC (87 $mV_{Ag/AgCl}$). The main difference between unsensitised and the sensitised Alloy 926 is the presence of chromium carbides in the second one. According to one of the theories about the causes of intergranular corrosion, the concentration of chromium in the precipitated carbides is much higher than in the surruounding matrix [44, 49, 51].

Therefore, chromium carbides are more cathodic than the rest of the surface. Then, it is probable that the potential of the galvanic pair between the carbides and the rest of the surface could be more positive than the surface without carbides.

The OCP values shift towards more positive values with temperature in both materials. This displacement is justified by the passive nature of Alloy 926. It is well known that temperature favours the kinetics of the corrosion reactions [52-55]. However, it also promotes the fast growth of the passive films on metallic surfaces [35, 56-58], which results in the ennoblement of the metal.

A slight trend to shift to more noble OCP values with immersion time is generally observed in unsensitised and sensitised Alloy 926, showing the properties of the passive films formed on the electrode surface during immersion in the LiBr solution.

3.4 Cyclic potentiodynamic curves

The cyclic potentiodynamic curves of unsensitised and sensitised Alloy 926 in 992 g/L LiBr solution were obtained at 25 ºC, 50ºC, and 75 ºC in order to evaluate the corrosion resistance of both materials at different temperatures.

3.4.1. Unsensitised Alloy 926

The cyclic potentiodynamic curves of unsensitised Alloy 926 in the 992 g/L LiBr at the different temperatures are shown in Figure 5.

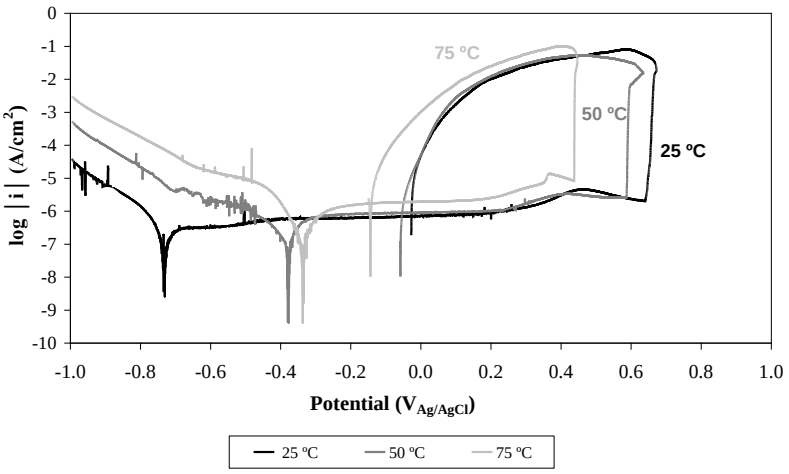

Figure 5. Cyclic Potentiodynamic curves for unsensitised Alloy 926 in the 992 g/L LiBr solutions at different temperatures.

Temperature affects the cathodic branch and all the values of current density along this branch increase with temperature. Unsensitised Alloy 926 shows a passivation behaviour at all the solution temperatures.

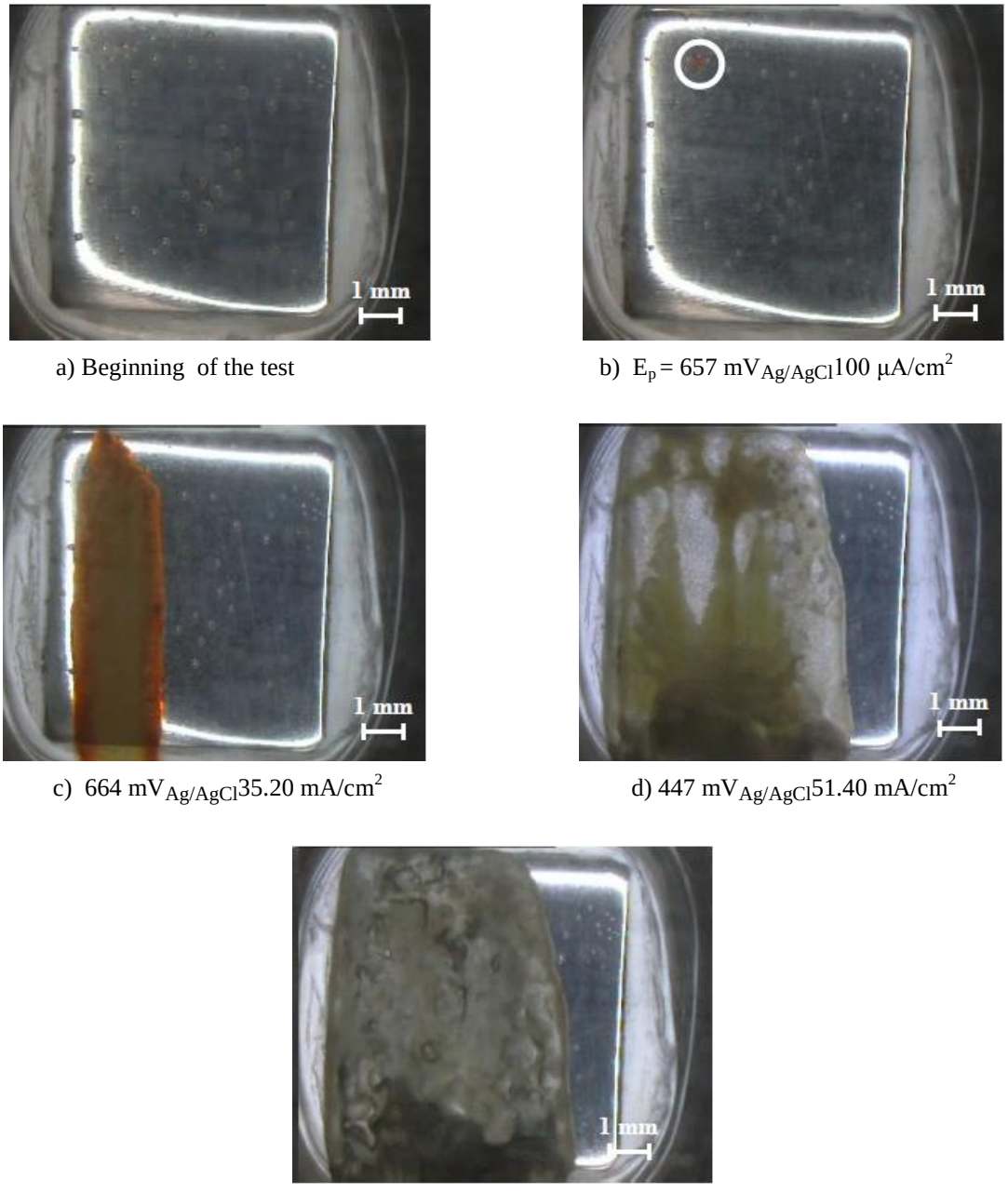

a) Beginning of the test

b) E_p = 657 $mV_{Ag/AgCl}$ 100 $\mu A/cm^2$

c) 664 $mV_{Ag/AgCl}$ 35.20 mA/cm^2

d) 447 $mV_{Ag/AgCl}$ 51.40 mA/cm^2

e) End of the test E_{rp} = - 17 $mV_{Ag/AgCl}$ 0.71 $\mu A/cm^2$

Figure 6. Images of the unsensitised Alloy 926 surface in the 992 g/L LiBr solution at 25 ºC at different moments of the cyclic potentiodynamic test. The first pit that appears on the surface during the pitting potential is marked with a white circle.

The range of the passivation zone decreases as the solution temperature increases: 1389 mV at 25 ºC, 967 mV at 50 ºC, and 776 mV at 75 ºC. The corrosion potential value shifts towards more

positive values as temperature increases. On the other hand, the pitting potential value decreases with the solution temperature, as shown in Figure 5. An anodic peak appears close to the pitting potential, these peaks appear at the same potential (around 300 $mV_{Ag/AgCl}$) at all temperatures and their potential interval is lower as the solution temperature increases.

These peaks are probably related to the region of transpassivity, where the Cr^{3+} ions in passive oxide layer for instance in the stainless steel begin to oxidize to soluble Cr^{6+}. It causes the passivity to breakdown and the current rise rapidly [59].

Figure 6 shows electrode surface images obtained at different moments of the electrochemical test in the 992 g/L LiBr solution at 25 ºC. The attack morphology at the other testing temperatures (50 and 75 ºC) is similar to this temperature. Figure 6 a) shows the aspect of the unsensitised Alloy 926 surface at the beginning of the test. Figure 6 b) shows the pitting potential (when current density reaches 100 $\mu A/cm^2$) of unsensitised Alloy 926 and how corrosion begins at a localised point of the electrode surface (marked with a white circle). Corrosion affects a large area of the electrode surface during the hysteresis loop, as shown in Figures 6 c), d), and e). Figure 6 d) shows a point of the hysteresis loop and Figure 6 e) shows the end of the test, when the repassivation potential is reached. At this point, only a small area of the electrode surface remains unaffected.

3.4.2. Sensitised Alloy 926

Figure 7 shows the cyclic potentiodynamic curves of sensitised Alloy 926 in the 992 g/L LiBr solution at different solution temperatures. All current density values of the cathodic branch increase as temperature increases.

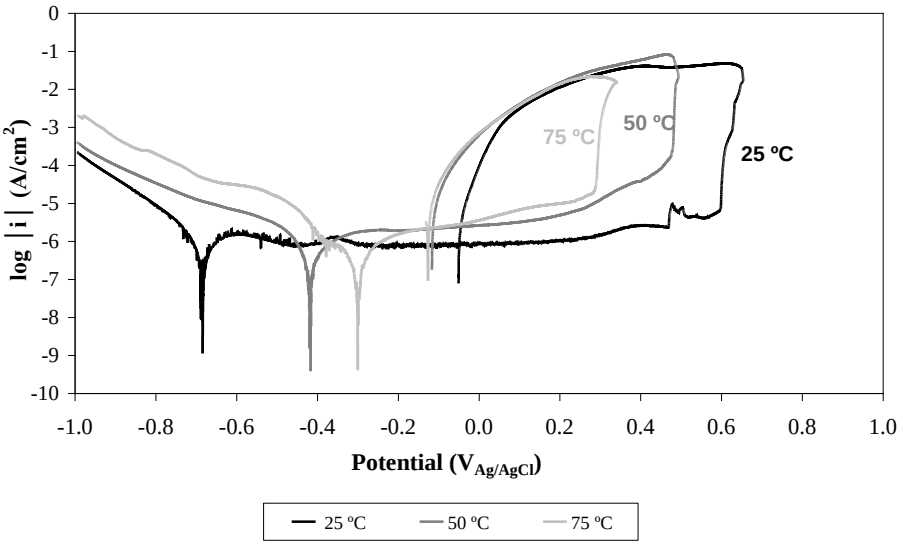

Figure 7. Cyclic Potentiodynamic curves for sensitised Alloy 926 in the 992 g/L LiBr solutions at different temperatures.

The current density of the anodic branch increases with temperature, too. The corrosion potential values shift towards more positive values with temperature and the pitting potential decreases. In the case of sensitised Alloy 926, the anodic peak only appears at 25 ºC; at higher solution temperatures (50 ºC and 75 ºC) current density goes on increasing during the passivation interval until the pitting potential is reached.

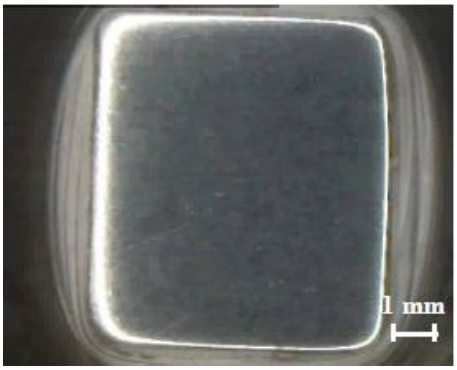

a) Beginning of the test

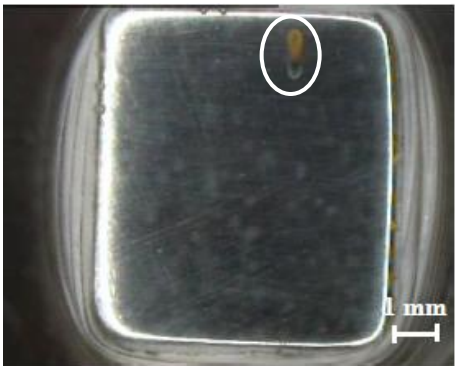

b) E_p = 606 $mV_{Ag/AgCl}$ 100 $\mu A/cm^2$

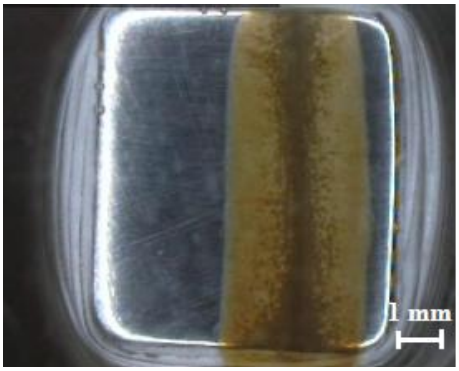

c) 647 $mV_{Ag/AgCl}$ 13.55 mA/cm^2

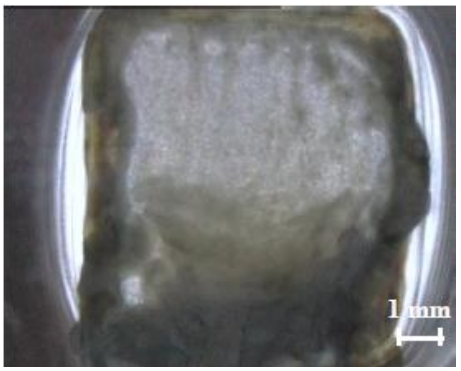

d) 381 $mV_{Ag/AgCl}$ 38.74 mA/cm^2

e) End of the curve E_{rp} = - 49 $mV_{Ag/AgCl}$ 0.674 $\mu A/cm^2$

Figure 8. Images of the sensitised Alloy 926 surface in the 992 g/L LiBr solution at 25 ºC at different moments of the cyclic potentiodynamic test. The first pit that appears on the surface during the pitting potential is marked with a white circle.

Images of the electrode surfaces obtained during the electrochemical test at 25 ºC are shown in Figure 8. Figure 8 a) shows an image of the sensitised Alloy 926 surface before the test. In this image, the electrode surface is completely unaffected. Figure 8 b) shows the electrode surface when pitting potential is reached. Like in the unsensitised sample, corrosion begins at a localised point. When the corrosion has begun, corrosion affects the entire electrode surface, as shown in Figures 8 c), d), and e). During the hysteresis loop (Figure 8d)), the entire surface is affected. At the end of the test the corrosion product completely covers the electrode surface (Figure 8 e)), when the repasivation potential is reached.

According to the attack morphology, first, corrosion appears as localised areas, from those localised points the corrosion process spreads over the entire surface during the hysteresis loop favoured by the corrosion product that catalyses the new corrosion reactions. This behaviour has been observed in other works [60-62]. The attack morphology is the same for the unsensitised and sensitised material at all temperatures.

From the cyclic potentiodynamic curves, the different electrochemical parameters: (corrosion potential (E_{corr}), corrosion current density (i_{corr}), pitting potential (E_p), passivation current density (i_p), and repassivation potential (E_{rp}) have been obtained for the different temperatures and materials (Table 1). The most precise determination of the corrosion current density values is by the Tafel extrapolation when both the anodic and cathodic branches show linearity. In the present study, some of the potentiodynamic curves did not show that necessary linearity. In those cases corrosion current densities were determined by the intersection of the cathodic Tafel line with the corrosion potential [63].

Table 1. Values of the corrosion potential (E_{corr}), corrosion current density (i_{corr}), pitting potential (E_p), passivation current density (i_{pas}), repassivation potential (E_{rp}) and repassivation current density (i_{rp}) for unsensitised and sensitised Alloy 926 in the 992 g/L LiBr solution at the different test temperatures.

Unsensitised Alloy 926						
T (ºC)	E_{corr} ($mV_{Ag/AgCl}$)	i_{corr} ($\mu A/cm^2$)	E_p ($mV_{Ag/AgCl}$)	i_{pas} ($\mu A/cm^2$)	E_{rp} ($mV_{Ag/AgCl}$)	i_{rp} (A/cm^2)
25	- 732	0.14	657	0.65	- 27	0.08
50	- 378	0.15	589	0.90	- 58	0.05
75	- 388	0.16	438	1.02	- 141	0.10

Sensitised Alloy 926						
T (ºC)	E_{corr} ($mV_{Ag/AgCl}$)	i_{corr} ($\mu A/cm^2$)	E_p ($mV_{Ag/AgCl}$)	i_{pas} ($\mu A/cm^2$)	E_{rp} ($mV_{Ag/AgCl}$)	i_{rp} (A/cm^2)
25	- 679	0.32	615	0.90	- 55	0.05
50	- 416	0.43	486	2.51	- 116	0.08
75	- 300	0.45	296	2.55	- 124	0.02

3.5. Corrosion potential and corrosion current density

Figure 9 shows the trend of the corrosion potential and corrosion current density values with temperature for unsensitised and sensitised Alloy 926 in the 992 g/L LiBr solution.

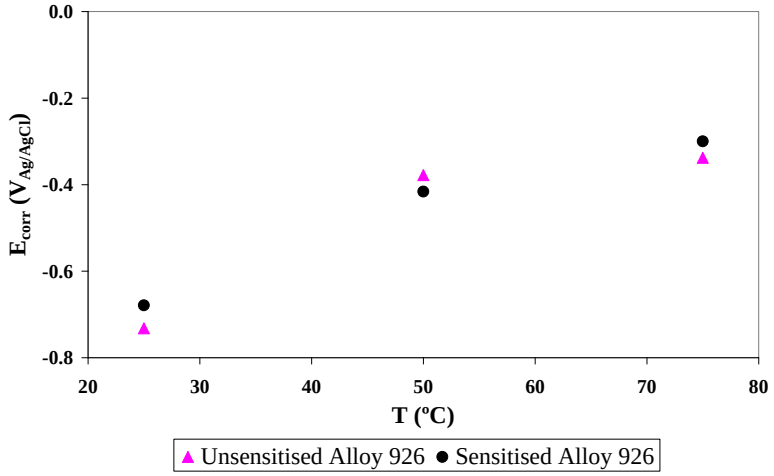

a) Corrosion potential values

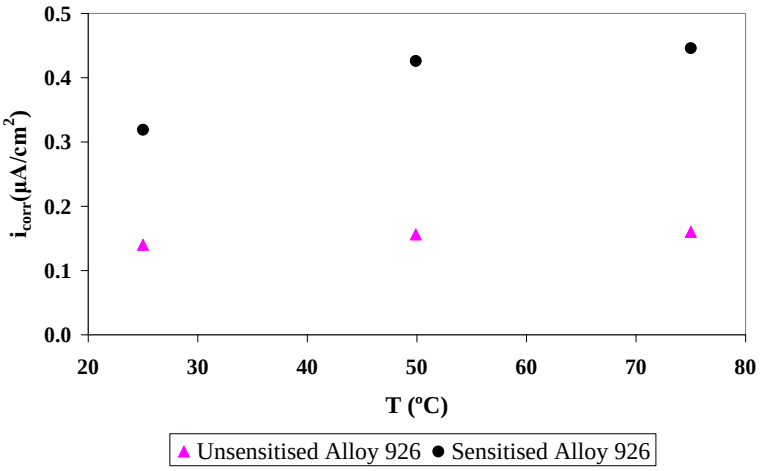

b) Corrosion current density values

Figure 9. Corrosion potential (a) and Corrosion current density (b) values of unsensitised and sensitised Alloy 926 in the 992 g/L LiBr solution at different temperatures.

The corrosion potentials present a clear trend to increase with temperature. This increase is more noticeable between the temperature of 25 ºC and 50 ºC. Corrosion potential values of unsensitised and sensitised Alloy 926 are similar.

The corrosion current density values of the unsensitised specimen are lower than the values obtained for sensitised Alloy 926 at all the solution temperatures. Furthermore, the corrosion current density values of the sensitised specimen increase with the solution temperature, being constant for the

unsensitised specimen. All this indicates that the sensitisation process affects the corrosion of Alloy 926, because despite the fact that the two specimens have a similar corrosion potential, sensitised Alloy 926 shows higher corrosion current densities at all temperatures and corrosion current density is related to the corrosion rate of metals. This result is similar to those reported by other researchers for sensitised steels in other solutions [64-68].

The increase in the corrosion potential with temperature seems to be related to the increase in the cathodic current density with temperature. In this way, the corrosion potential shifts toward more positive values. The trend in the corrosion potential with temperature is similar to the trend in the OCP values.

3.6. Pitting corrosion susceptibility

Pitting potential and passivation current density values are represented in terms of the solution temperature in Figure 10**.**

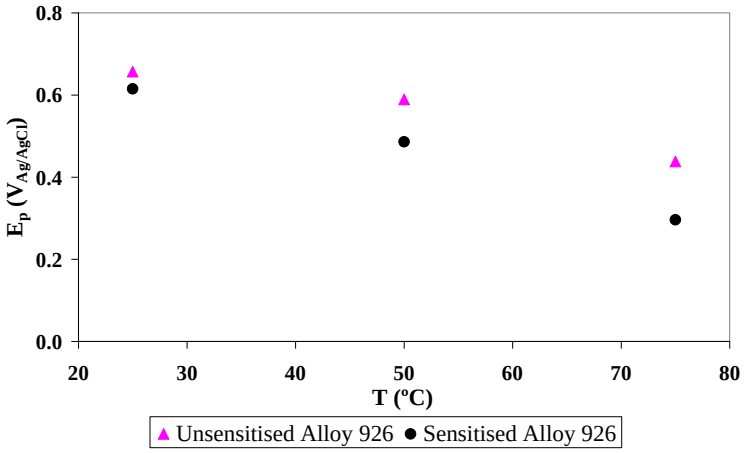

a) Pitting potential values

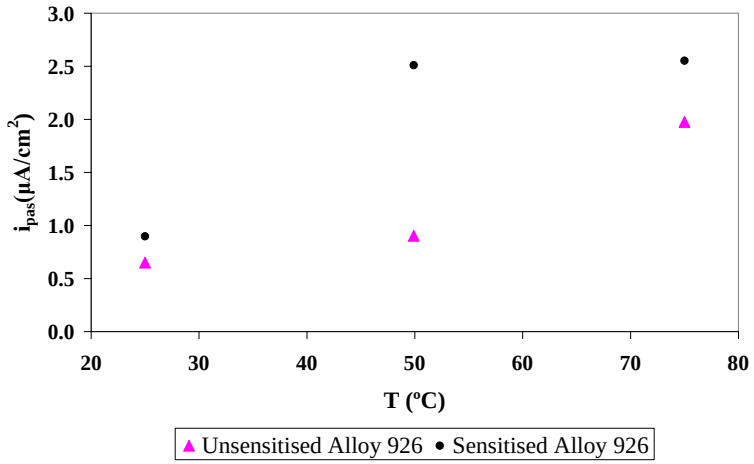

b) Passivation current density values

Figure 10. Pitting potential (a) and passivation current density values (b) of unsensitised and sensitised Alloy 926 in the 992 g/L LiBr solution at different temperatures.

The pitting potential is higher for the unsensitised sample than for the sensitised sample. The pitting potential represents the potential limit above which the formation of stable pits begins [53]. It is generally agreed that the more noble the value of the pitting potential, the more resistant the metal is to pit initiation. Therefore, the localised corrosion resistance drops if Alloy 926 is heated at 825 ºC for one hour. Consequently the overall resistance to pitting of Alloy 926 was degraded with heat treatment. On the other hand, the pitting potential values diminish with the solution temperature, and this decrease is higher in the sensitised specimen.

Unsensitised and sensitised Alloy 926 present a clear passivation range under all the studied conditions. During the passivation range the corrosion rate was determined by the passivation current densities, selecting the same potential of the passivation interval (perfect passivity zone) for each test and checking the current density value at this point. The results show that passivation current density values are higher for sensitised Alloy 926 than for the unsensitised specimen, and that passivation current density increases with temperature.

The increase in the passivation current density and the drop in the pitting potential as a consequence of the heat treatment are in agreement with the results obtained in the sensitisation characterisation. These results indicated that the chromium carbides observed in the microscopic analysis cause the chromium depletion in the areas close to precipitates and subsequently a weaker passive film. The differences in the passivation current density are mainly attributable to the difference in the minimum level of chromium of depletion zones [10]. These results are similar to those reported by other authors for sensitisation processes in other steels [65-67, 69, 70].With regard to the solution temperature, the results reveal that the properties of the passive film can be degraded as temperature increases. Temperature favours the activity of aggressive anions. Moreover, temperature decreases the protective properties of the film. Researchers propose two reasons for this behaviour [71]: a) the porosity of the passive film increases with temperature, b) the passive film undergoes an intrinsic modification of its chemical composition and/or physical structure. The passive film degradation is observed in the pitting potential drop and the passivation current density increment. Unsensitised and sensitised Alloy 926 are less generalised and localised corrosion resistant as temperature increases. This influence of the temperature on the corrosion behaviour of Alloy 926 seems similar to that reported by other authors for halide pitting in stainless steels [36, 53, 55, 57, 72].

3.7. Repassivation behaviour

Figure 11 shows the perfect (E_{rp} - E_{corr}) and imperfect (E_p – E_{rp}) passivity intervals, furthermore the OCP are indicated over the passivity intervals for every test. The (E_{rp} – E_{corr}) difference was defined as the perfect passivation zone according to Bellezze [73]. Between these potential values pitting corrosion will not initiate and existing pits will not propagate. This difference is lower in sensitised Alloy 926 than in unsensitised Alloy 926. In addition to this, the difference is lower as temperature increases. The values obtained from the (E_p – E_{rp}) difference, defined as the imperfect passivity zone [73], are a measure of the trend of nucleated pitting growth. The trend of the pitting potential values is to decrease as a consequence of heat treatment and temperature. Hence, the

imperfect passivity zone is larger in the unsensitised specimen than in the sensitised specimen at all temperatures.

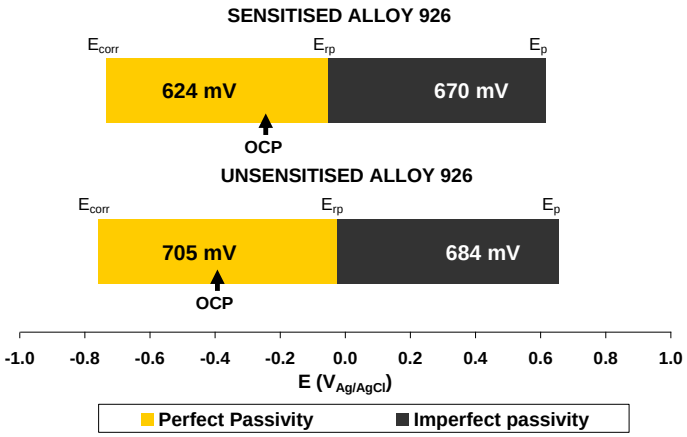

a) 25 ºC

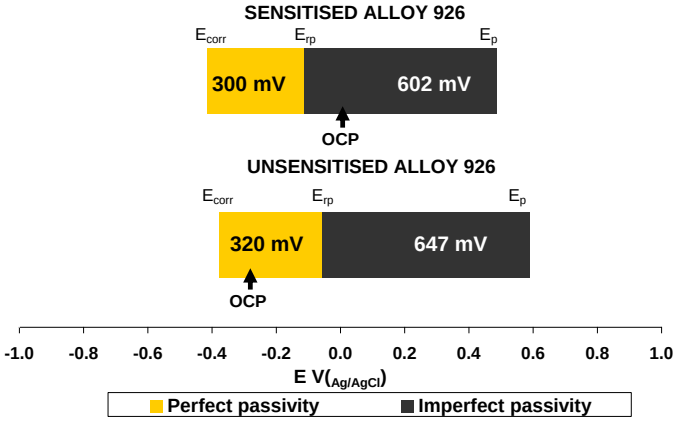

b) 50 ºC

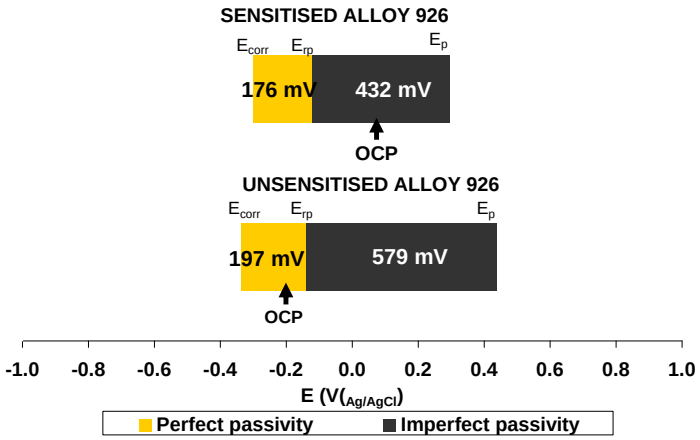

c) 75 ºC

Figure 11. Perfect (E_{rp} - E_{corr}) and imperfect passivity (E_p - E_{rp}) ranges for unsensitised and sensitised Alloy 926 in the 992 g/L LiBr solution at the different temperatures. The OCP values are marked over the passivation range.

The repassivation potential values are more noble than the corrosion potentials for unsensitised and sensitised Alloy 926 at all temperatures. The repassivation potential is slightly higher for unsensitised Alloy 926 at 25 ºC and 50 ºC than for the sensitised sample and it is similar at 75 ºC. On the other hand, the repassivation potential decreases with temperature. All the materials exhibit hysteresis loop, as shown in Figures 5 and 7. Hence, if an eventual breakdown of the passive film happens, both materials are able to regenerate it.

Alloy 926 is passivated in the studied LiBr solution at 25 ºC, 50 ºC, and 75 ºC, since the OCP (Figure 4) values are in the passive zone of the potentiodynamic curves (Figures 5 and 7). Furthermore, the OCP values are more positive than their corrosion potential values and less positive than the repassivation potential values for the unsensitised sample at all temperatures. However, in the sensitised sample, OCP values present a trend to go in the imperfect passivity zone as the solution temperature increases. The sensitised sample shows higher OCP values than the repassivation potential at 50 ºC and 75 ºC. These facts mean that under open circuit conditions, only in the sensitised sample at 50 ºC and 75 ºC existing pits could propagate.

4. CONCLUSIONS

The conclusions of this research may be summarised as follows:

1. Alloy 926 heated at 825 ºC during 1 hour undergoes chromium carbide precipitation in the grain boundaries. These carbides are revealed by the etching with oxalic acid or are observed by SEM analysis and backscattered electrons.
2. The precipitation of chromium carbides produces chromium depletion in the adjacent areas and the heated Alloy 926 becomes sensitised to intergranular corrosion. This sensitisation can be characterised by means of the electrochemical reactivation tests.
3. The open circuit potential of Alloy 926 in the 992 g/L LiBr solution increases as a consequence of the heat treatment and the solution temperature.
4. The cathodic current density of the potentiodynamic curves of Alloy 926 in the 992 g/L LiBr solution increases with temperature, that is, the cathodic reaction rate, which shifts the corrosion potential to higher values with temperature. On the other hand, the values of the cathodic current density between unsensitised and sensitised Alloy 926 are similar, it being only slight greater for the sensitised sample at 25 ºC.
5. The corrosion current density is higher in the sensitised specimen than in the unsensitised one. Therefore, sensitised Alloy 926 is less corrosion resistant. The corrosion current density increases with the solution temperature in both unsensitised and sensitised Alloy 926
6. Unsensitised and sensitised Alloy 926 show a passive behaviour in the 992 g/L LiBr solutions. Both alloys can repassivate after the breakdown of the passive film.
7. The pitting potential of Alloy 926 in the 992 g/L LiBr solution is less noble in the sensitised material than in the unsensitised material and decreases with temperature. On the other hand, the passivation current density is higher for the sensitised specimen. Then, the sensitisation process

produces a weaker passive film and reduces resistance to localised corrosion. The passivation current density increases with the solution temperature in both unsensitised and sensitised Alloy 926

8. The corrosion attack begins in localised zones, but during the hysteresis loop corrosion damage affects the electrode surface in a generalised way.

ACKNOWLEDGEMENTS
We wish to express our gratitude to MICINN (CTQ2009-07518), to FEDER, to Dr. Helena Alves from Krupp VDM for supplying the materials, and to Dr. Asunción Jaime for her translation assistance.

References

1. Council Decision of 14 October 1988 concerning the conclusion of the Vienna Convention for the protection of the ozone layer and the Montreal Protocol on substances that deplete the ozone layer, Official Journal L 297, 31/10/1988 p. 8-28.
2. http://unfccc.int, website of United Nations Framework Convention on Climate Change. (2010).
3. K. Tanno, M. Itoh, T. Takahashi, H. Yashiro, N. Kumagai. *Corros. Sci*. 34 (1993) 1441.
4. J.W.Furlong. *The Air Pollution Consultant* 11/12. (1994), 1.12-1.14.
5. Y.F.Cheng, J. L. Luo. *Electrochimica Acta* 44 (1999) 4795.
6. Jae-Bong Lee. Mater. *Chem. Phys*. 99 (2006) 224.
7. M.J. Carmezim, A.M. Simoes M.F. Montemor, M. Da Cunha Belo. *Corros. Sci*. 47 (2005) 581.
8. Martin Matula, Zuzana Stonawska, Ludec Tuma, Catherine Dagbert, Ludmila Hyspecka, Jacques Galland. Electrochemical testing of sensitization to intergranular corrosion in stainless steel. Eurocorr 2001, Riva del Garda (Italia) (2001).
9. O.Greven, H.-E Bühler, L.Gerlach. Corrosion investigations on chemical resistant steels by means of the potenciostatic electrochemical reactivation test (ERT). Eurocorr 2001, Riva del Garda (Italia) (2001).
10. V. Kain, R.C. Prasad, P.K. De. *Corrosion* 58 (2002), 15.
11. Z. Fang, Y.S. Wu, L. Zhang, J.Q. Li. *Corrosion* 54 (1998), 339.
12. P. Muraleedharan, J.B. Gnanamoorthy, P. Rodriguez. *Corrosion 5*2 (1996) 790.
13. Martin Matula, Ludmila Hyspecka, Milan Svoboda, Vlastimil Vodarek, Catherine Dagbert, Jacques Galland, Zuzana Stonawska, Ludec Tuma. *Mater. Charact*. 46 (2001) 203.
14. H.-E Bühler, L. Gerlach, O. Greven, W. Bleck. *Corros. Sci*. 45 (2003) 2325.
15. Shenghan Zhang, Toshio Shibata, Takumi Haruna. *Corros. Sci*. 47 (2007) 1049.
16. AnKe Hempsch, G. Schmitt, W.Blek. Advances in assessing the susceptibility to intergranular corrosion (IGC) of duplex stainless steel using the electrochemical reactivation test (ERT). Eurocorr 2006, Maastricht (Netherlands) (2006).
17. G.H. Aydogdu, M.K. Aydinol. *Corros. Sci*. 48 (2006) 3565.
18. H. Shaikh, N. Sivaibharasi, B. Sasi, T. Anita, R. Amirthalingam, B.P.C. Rao, T. Jayakumar, H.S. Khatak, Baldev Raj. *Corros. Sci*. 48 (2006) 1462.
19. V.Kain, K.Chandra, K.N.Adhe, P.K.De. *Corrosion* 61 (2005) 587.
20. A.S. Lima, A.M. Nascimento, H.F.G. Abreu, P. De Lima-Neto. *J. Mater. Sci*. 40 (2005) 139.
21. T. Amadou, C. Brahan, H. Sidhom. *Metall. Mater. Trans. A-Phys. Metall. Mater. Sci*. 35A (2004) 3499.
22. N. Parvathavarthini, R. K. Dayal. *J. Nucl. Mater*. 399 (2010) 62.
23. Xiaofei Yu, Shenhao Chen, Ying Liu, Fengfeng Ren. *Corros. Sci*. 52 (2010) 1939.
24. K.O.E. Henriksson, N. Sandberg, J. Wallenius. *Appl. Phys. Lett.* 93 (2008) 191912 .
25. M. Detroye, F. Reniers, C. Buess-Herman, J. Vereecken. *Appl. Surf. Sci*. 144-145 (1999) 78.

26. ASTM international. ASTM A -262. Standard Practices for Detecting Susceptibility to Intergranular Attack in Austenitic Stainless Steels (2004).
27. V. Cihal, A. Desestret, M. Froment, G.H. Wagner, Étude de nouveaux tests potentiocinétiques de corrosion intergranulaire des aciers inoxydables, Étude CETIM, Center de Recherches de Firminy, C.A.F.L., Rapport N, 958, 1969.
28. Nathalie Lopez, Mariano Cid, Monique Puiggali, Iñaki Azkarate, Alberto Pelayo. *Mater. Sci. Eng. A-Struct. Mater. Prop. Microstruct. Process*. A 229 (1997) 123.
29. M. Akashi, T. Kawamoto, F. Umemura, B. Gijutsu, *Corros. Eng*. 29 (1980) 163.
30. ASTM international. ASTM G - 108 Standard Test method for electrochemical reactivation for detecting sensitization of AISI 304 y 304L stainless steels. (2004).
31. E. Sarmiento, J.G. Gonzalez-Rodriguez, J.Uruchurtu, O. Sarmiento, M. Menchaca. *Int. J. Electrochem. Sci*. 4 (2009) 144.
32. E. Blasco-Tamarit, A. Igual-Muñoz, J. Garcia-Antón, D. García-García. *Corros. Sci*. 48 (2006), 863.
33. A.Igual Muñoz, J. García-Anton, J.L. Guiñon, V. Pérez-Herranz. *Corros. Sci*. 49 (2007), 3200.
34. A.Igual Muñoz, J. García-Anton, J.L. Guiñon, V. Pérez-Herranz. *Electrochim. Acta* 50 (2005) 957.
35. M.J. Muñoz-Portero, J. García-Anton, J.L. Guiñon, V. Pérez-Herranz. *Pasivation of metals and semiconductors and properties of thin oxide layers*. (2006) 131.
36. E. Blasco-Tamarit, A. Igual-Muñoz, J. Garcia-Antón, D. García-García. *Corros. Sci*. 50 (2008) 1848.
37. E. Blasco-Tamarit, A. Igual-Muñoz, J. Garcia-Antón, D. García-García. *Corros. Sci*. 49 (2007), 1000.
38. M.T. Montañés, R. Sánchez-Tovar, J. García-Antón, V. Pérez-Herranz. *Int. J. Electrochem. Sci*. 5 (2010) 1934.
39. R. Leiva-Garcia, M.J. Muñoz-Portero, J. Garcia-Anton. *Corros. Sci*. 52 (2010) 950.
40. R. Leiva-Garcia, M.J. Muñoz-Portero, J. Garcia-Anton. *Corros. Sci.* 51 (2009) 2080.
41. R. Leiva-Garcia, M.J. Muñoz-Portero, J. Garcia-Anton. Comparative study of electrochemical methods and image analysis for the characterization of Alloy 146, 279, 900, and 926 sensitization to intergranular corrosion. Eurocorr 2008, Edinburg (United Kingdom) (2008).
42. C.J. Park, V. Shankar Rao, H.S. Kwon. *Corrosion* 61 (2005) 76.
43. K.N. Adhe, V. Kain, K. Madangopal, and H.S. Gadiyar. *J. Mater. Eng. Perform*. 5 (2007) 500.
44. V. Cihal, *Intergranular corrosion of steels and alloys, Elsevier, Amsterdam*, (1984).
45. J. Garcia-Anton, A. Igual Muñoz, J.L. Guiñon, V. Perez Herranz. Electro-Optical Method by On-line Visualization of Electrochemical Process and Experimental Process. Spain P-200002525 (2000).
46. J. Garcia-Anton, A. Igual Muñoz, J.L. Guiñon, V. Perez Herranz. Horizontal Electrochemical Cell by the Electro-Optical Analysis of Electrochemical Process. Spain P-200002526 (2000).
47. J. Garcia-Anton, A. Igual Muñoz, J.L. Guiñón, and V. Perez Herranz. *J. Appl. Electrochem*. 31 (2001) 1195.
48. J. Garcia-Anton, A. Igual Muñoz, J.L. Guiñón, V. Perez Herranz, J. Pertusa-Grau. *Corrosion* 59 (2003) 172.
49. Otero Huerta. Corrosión y degradación de los materiales. *Ed. Sintesis*, (1997). 138-156.
50. Metals Handbook, Ninth Edition: Volume 13 - *Corrosion* (ASM Handbook) [Hardcover] Lawrence J. Korb, ASM.
51. D.T.Llewellyn, Roger C. Hudd. Steels: metallurgy and applications. Butterworth-Heinemann (1998).
52. A.Igual Muñoz, J. García-Antón, S.Lopez Nuévalos, J.L. Guiñón, V. Perez Herranz. *Corros. Sci.* 46 (2004) 2955.
53. A.Pardo, E. Otero, M.C. Merino, M.D. Lopez, M.V. Utrilla, F. Moreno. *Corrosion* 56 (2000) 411.
54. L.F. Garfias-Mesias, J. M.Sykes. *Corros. Sci*. 41 (1999) 959.

55. N.J. Laycock. *Corrosion* 55 (1999) 590.
56. T. Laitinen, N. Bojinov, I. Betova, K. Mäkelä, T. Saario. STUK (Radiation and nuclear safety authority) (1999), 1-75.
57. D.H. Hur, Y.S. Park. *Corrosion* 62 (2006) 745.
58. C.O.A. Olsson and D. Landolt. *Electrochim. Acta* 48 (2003) 1093.
59. P. Záhumenský, S. Tuleja, J. Országová, J. Janovec, V. Siládiová. *Corros. Sci*. 41 (1999) 1305.
60. R. Leiva-García, J. Garcia-Anton, M.J. Muñoz-Portero. *Corros. Sci*. 52 (2010) 2133.
61. M M. Dornhege, C. Punckt, J.L. Hudson, H.R. Rotermund. J. Electrochem. Soc. 154 (2007), C24.
62. B. Wu, J.R. Scully, J.L. Hudson, A.S. Mikhailov. J. Electrochem. Soc. 144 (1997) 1614.
63. E. McCafferty. Corros. Sci. 47, (2005), 3202.
64. T. Poormina, Jagannath Nayak, A.Nityananda Shetty. *Int. J. Electrochem. Sci*. 5 (2010) 56.
65. A.S.M. Paroni, N. Alonso-Falleiros, R. Magnabosco. *Corrosion 6*2 (2006) 1039.
66. R.F.A. Jargelius Petterson. *Isij International* 36 (1996) 818.
67. P. Záhumensky, S. Tuleja, J. Országova, J. Janovec, V. Magula. *Corrosion* 57 (2001) 874.
68. H. Shaikh, G. George, F. Shneider, K. Mummert, H.S. Khatak. Transactions of the Indian Institute of Metals 54 (2001) 27.
69. Wen-Ta Sai, Chi-Lu Yu, Jeih-Ing Lee. *Scripta mater*. 53 (2005), 505.
70. Ching-An Huang, Yau-Zen Chang, S.C. Chen. *Corros. Sci*. 46 (2004) 1501-1513.
71. J.H. Wang, C.C. Su, and Z. Szklarska-Smialowska. *Corrosion* 44 (1988) 732.
72. R.M. Carranza, M.G. Alvarez. *Corros. Sci*. 38 (1996) 909.
73. T. Bezelle, G. Roventi, R. Fratesi. *Electrochim. Acta* 49 (2004) 3005